coatings

MDPI

Article

Laser Curing of Digitally Printed Polymer–Silver Composite Conductive Tracks on Polycarbonate Substrates

Jonas Mertin [1,*], Tamila Rozibakieva [1], Christian Vedder [1] and Jochen Stollenwerk [1,2]

[1] Fraunhofer Institute for Laser Technology ILT, 52074 Aachen, Germany
[2] Chair for Technology of Optical Systems TOS, RWTH Aachen University, 52074 Aachen, Germany
* Correspondence: jonas.mertin@ilt.fraunhofer.de

Abstract: In this article, we present an approach to fabricate conductive tracks on polymer substrates. Here, a digital printing process is used together with subsequent processing by a laser. For this purpose, a silver flake-based composite is printed onto a polycarbonate substrate using a jet-dispensing process. The printed tracks are then cured using a pyrometer-controlled laser beam source. The fabricated samples are analyzed for electrical resistivity and the cross-sectional area of the conductive tracks and compared to conventionally oven-cured samples. Four-point measurements and an optical measurement method are used for this purpose. Based on the resulting resistance, two different process regimes can be observed for the laser curing process. By using a laser instead of an oven for post-treatment, the achieved resistance of the conductive tracks can be reduced by a factor of 2. Moreover, the tracks produced in this way are more reproducible in terms of the resistance that can be achieved.

Keywords: printed electronics; composite coating; drop-on-demand printing; thick film technology; jet-dispensing; laser material processing; additive manufacturing

Citation: Mertin, J.; Rozibakieva, T.; Vedder, C.; Stollenwerk, J. Laser Curing of Digitally Printed Polymer–Silver Composite Conductive Tracks on Polycarbonate Substrates. *Coatings* **2023**, *13*, 10. https://doi.org/10.3390/coatings13010010

Academic Editors: Ana-Maria Mocioiu and Oana Catalina Mocioiu

Received: 28 November 2022
Revised: 15 December 2022
Accepted: 19 December 2022
Published: 21 December 2022

1. Introduction

The demand for functionally integrated components is growing across all industries [1,2]. Due to the increasing individualization of consumer products, the lot sizes of a single product variant are decreasing—for example, in the automotive sector [3,4]. Cable harnesses in the automotive industry are assembled individually per car, generating enormous costs. By using digital printing technologies, it is possible to automate and customize, e.g., signal cables, and apply them directly to components in a cost-effective manner down to a lot size of 1 [1,5]. Nevertheless, the necessary post-treatment of printed conductors remains a bottleneck in production. These must be conventionally post-treated in an oven at temperatures between 100 °C and 200 °C [6,7]. Since the substrate is heated accordingly, this process is disadvantageous in terms of energy efficiency [8,9]. Further, the substrates to be used are limited in terms of heat stability for post-treatment [10]. Alternative technologies for the thermal post-treatment of printed layers on components have various process-specific disadvantages: Intense Pulse Light (IPL), for example, is not suitable for thick layers due to its short pulse duration, the near-surface absorption for thick layers >>1 µm and for processing 3D components due to the radiation characteristics of the energy source [11–13]. By using a laser beam for the thermal treatment of printed structures, various disadvantages of other technologies can be sidestepped: the selective, localized application of energy means that less energy is required for the thermal processing of printed structures, the thermal impact on the substrate is reduced, and the 3D capability of the process is ensured by using appropriate positioning systems (3–5-axis machines, robots or scanning systems) [8,11,13,14]. This approach, combined with a digital printing technology for digital, selective coatings, enables the fabrication of electrically conductive structures on a wide range of substrates [12,14–19].

In this work, we use a combination of jet dispensing and laser treatment to apply conductive traces directly to a polycarbonate surface. The process is designed to be 3D-capable as well as scalable and cost-efficient.

2. Materials and Methods

2.1. Substrate and Paste

Plates composed of polycarbonate (PC, "LD50" white, light transmission 50%, KTK Kunststofftechnik Vertriebs GmbH, Germering, Germany) were used as a substrate for the conducted experiments. These were cut to a size of 150 × 150 × 3 mm^3 for easier handling in the machines used.

Screen printing paste "1901-SB" (Ferro GmbH, Hanau, Germany) was used as the paste to print the conductive tracks. The main components of the paste were silver flakes and butyl diglycol acetate. Under the influence of heat, the butyl diglycol acetate polymerized as a matrix around the silver flakes, and electric current flow either by percolation or by contact of the silver flakes was possible. For this reason, the paste consisted of both small, approximately spherical flakes and large, irregularly shaped flakes (cf. Figure 1). Since this paste had a very high viscosity and was very thixotropic as a material for screen printing, it was diluted for printing with a jet dispenser. For this purpose, "Thinner 401" (Ferro GmbH, Hanau, Germany) was added, with a mass fraction of 1 wt.%; the material mixture was homogenized with a spatula and filled into a 5CC cartridge.

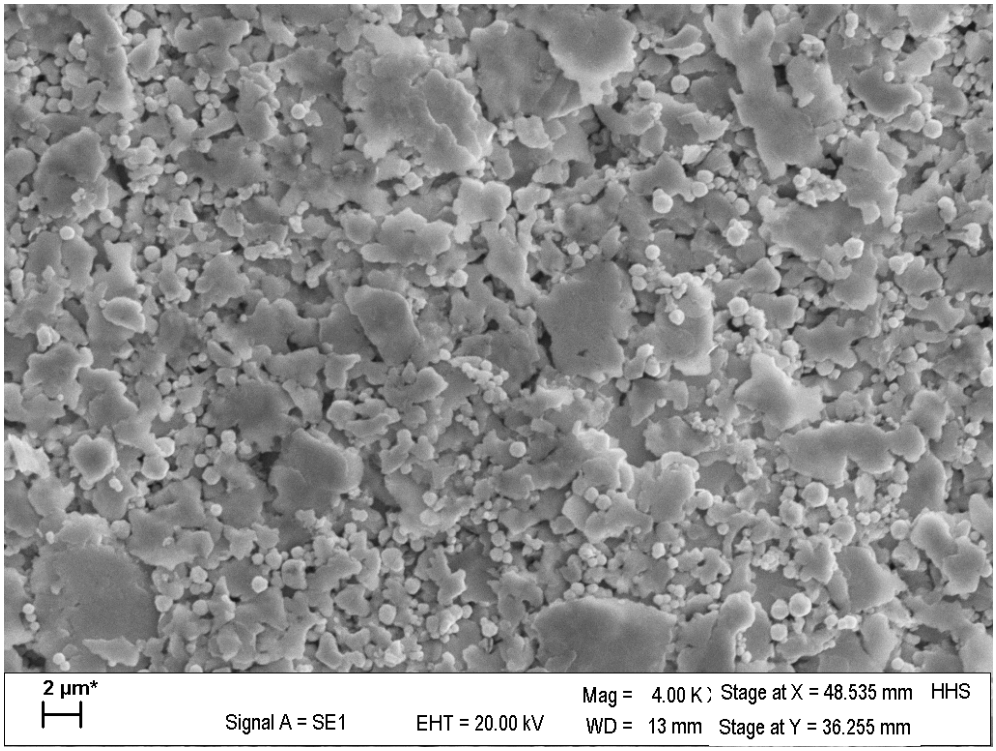

Figure 1. Scanning electron microscope (SEM) picture of the silver flakes used in the paste. The paste consists of small, almost spherical flakes, as well as large irregularly shaped flakes. All flakes consist of pure silver. For sample preparation, the components of the paste were separated using a centrifuge. The remaining flakes then were deposited onto a silicon wafer for SEM characterization.

2.2. Sample Preparation

A jet dispenser type "MDV 3200 A-HS" (Vermes Microdispensing GmbH, Holzkirchen, Germany) equipped with a nozzle (diameter 100 µm) was used to prepare the samples. The material placed in the 5CC cartridge was forced through the nozzle by compressed air and a piezo plunger, forming a droplet that was deposited on the substrate surface without machine contact.

The jet dispenser was mounted on a 3-axis machine (PFE 510-PX, BZT Maschinenbau GmbH, Leopoldshöhe, Germany) and computerized numerical control (CNC) was used to trigger the droplets. The upstream pressure in the cartridge was 2 bar and the distance between the sample surface and the nozzle was 2.5 mm. The width and cross-section of the traces were determined by the number of drops per unit length. In this work, 7 drops per second were deposited for the traces at a feed rate of 3 mm/s, resulting in a cross-section of the wet, untreated layer of approx. 0.055 mm^2 and a width around 0.75 mm. With this setup, 11 traces each with a length of 100 mm were deposited on each of the PC substrates (cf. Figure 2).

Figure 2. Photography of samples used: polycarbonate substrate with 11 printed conductive lines produced from silver paste 1901-SB. Length of each line is 100 mm, width of each line is approximately 0.75 mm, cross-section before curing is approximately 0.055 mm.

2.3. Curing of Samples by Laser Radiation

For the thermal post-treatment of the printed layers, they were locally irradiated with a laser beam. A diode laser (λ = 976 nm, P_L = 200 W, Dilas Diodenlaser GmbH, Mainz, Germany) was used for this purpose. Characterization of the laser power was performed using a power meter (Coherent PM300F-50 and Coherent PM30, Coherent Inc., Santa Clara, CA, USA). The laser beam was guided to an optical system by means of an optical fiber and focused by this system to a beam diameter of 1.2 mm (cf. Figure 3), measured by a beam characterization system ("FocusMonitor", PRIMES GmbH, Pflugstadt, Germany). Since the intensity distribution was not uniform, inhomogeneous heat input orthogonal to the feed direction of the laser beam was to be expected during machining. However, this circumstance was at least partially compensated by the likewise non-uniform cross-section of the conductor tracks (as seen in Section 3.4).

Since the beam diameter was larger than the width of the conductive tracks, a portion of the intensity was coupled into the substrate. Due to the scattering and non-absorbing properties of the PC substrates, there was no measurable impact on the substrate. In order to be able to use black substrates as well, the laser beam diameter would have to be adapted very precisely to the width of a single track.

In addition, the path of the laser beam was superimposed with the beam path of the pyrometrically measured heat radiation from the processing zone (pyrometer SE252, Amtron GmbH, Aachen Germany). Appropriate dichroic mirrors and a beam splitter were used for this purpose (cf. Figure 4). The pyrometric sensor measured the thermal radiation in a spectral range between 1.2 and 2.3 µm, with the sensitivity of the sensor

being highest between a wavelength of 1.8 and 2.2 µm. A proportional-integral-differential (PID) controller was used to adapt the laser power in order to achieve a set temperature within the processing zone (control temperature).

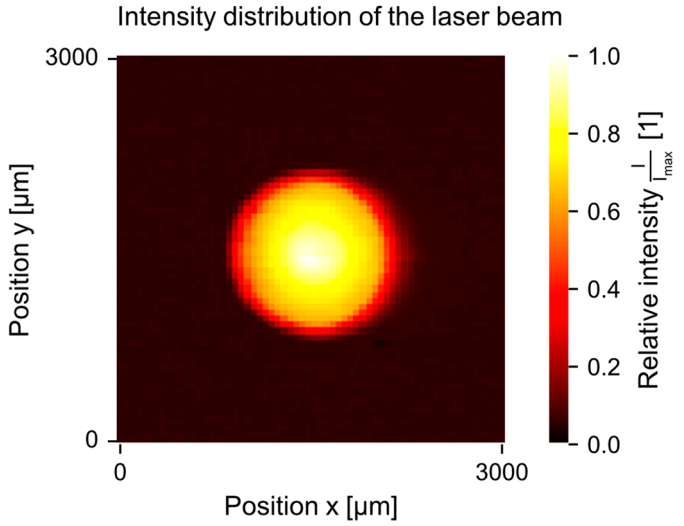

Figure 3. Intensity distribution of the laser beam used for the experiments performed in this work. The beam diameter according to the second-moment width is 1.2 mm.

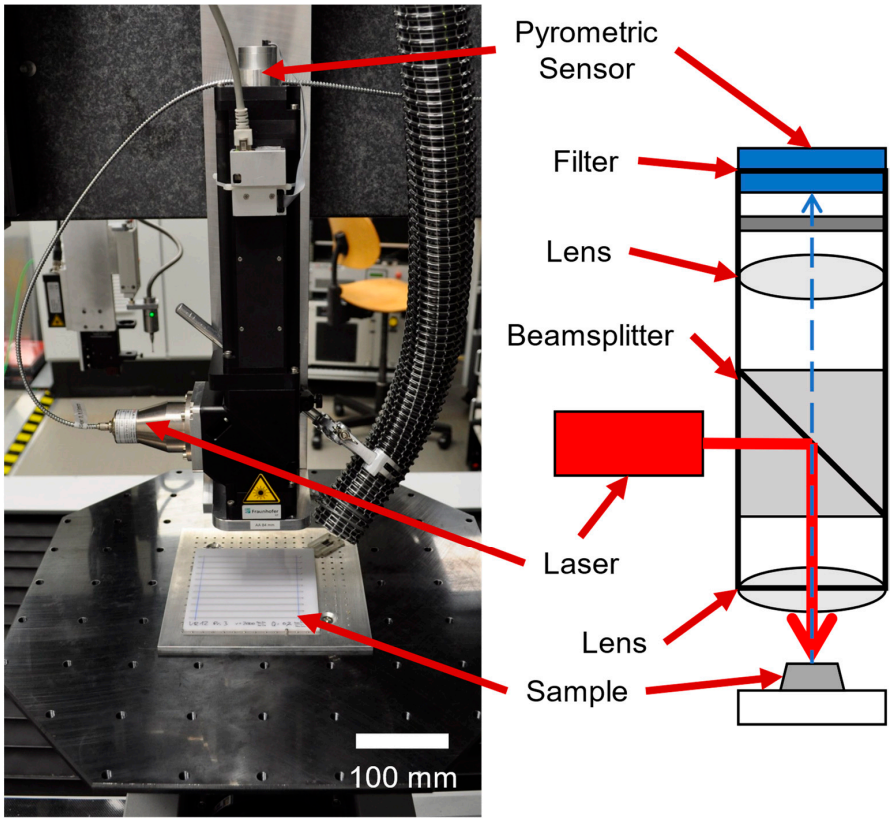

Figure 4. (**Left**): photography of the experimental setup used. (**Right**): schematic representation of the optical setup for laser beam as well as pyrometry.

A calibration curve was determined experimentally to compensate for the deviation between the target temperature and the real temperature of the layer: a sample (aluminum plate with a printed square of the paste on it) was heated with a hot plate (PZ 28-3T, Harry Gestigkeit GmbH, Düsseldorf, Germany) and the surface temperature was measured with a contact ther-

mometer (Fluke 52II, Fluke Deutschland GmbH, Glottertal, Germany) at the same time as the pyrometric signal. This was carried out for temperatures between 100 °C and 200 °C.

The optical setup was mounted on a 5-axis machine and the laser and pyrometer were controlled via the digital outputs of the CNC. For the tests performed, the traces were completely traversed twice at a feed rate of 1000 mm/min. Here, the control temperature was varied between 110 °C and 150 °C, and the temperature as well as the diode current of the laser was logged.

For reference, an additional sample was processed in an oven at a temperature of 125 °C for 30 min, which was the manufacturer's recommendation for curing.

2.4. Analysis of the Cured Samples

Both electrical resistivity and cross-section measurements were performed to analyze the fabricated samples. Four-wire measurements were performed to electrically characterize the samples. The electrical resistances of the individual samples were determined, the measurements of the same processing parameters were averaged, and the standard deviation was determined. To determine the cross-section of the conductive track, measurements using a laser scanning microscope (LSM) were executed. Therefore, a conductive track for each processing parameter was measured at three positions: around 10 mm after the start of the conductive track, in the middle and around 10 mm before the end of the conductive track. This was done to check for the homogeneity of the cross-section of the conductive track, as well as for the influence of the laser radiation.

3. Results

3.1. Calibration and Characterization of the Equipment Used

3.1.1. Characterization of the Laser Power Depending on the Current Setting of the Pyrometer

The optical power as a function of the diode current was measured and plotted (cf. Figure 5). Since there was a non-linear correlation between the optical power and the diode current set for a diode current smaller than 2% of the maximum current, two different functions were fitted for the data:

$$P(I) = \begin{cases} a_1 I + a_0 & I > 2\% \\ b_2 I^2 + b_1 I + b_0 & I \leq 2\% \end{cases} \quad (1)$$

This resulted in the following model function for the conversion of the laser data:

$$P(I) = \begin{cases} 1.559\ \frac{W}{\%} \cdot I - 1.998\ W & I > 2\% \\ 0.478\ \frac{W}{\%^2} \cdot I^2 - 0.380\ \frac{W}{\%} \cdot I + 0.087\ W & I \leq 2\% \end{cases} \quad (2)$$

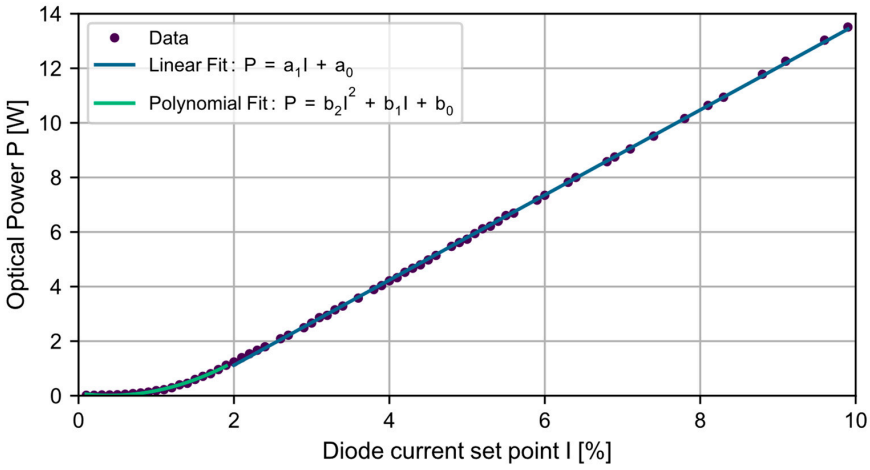

Figure 5. Measurement and fitted model for the correlation between the diode current set by the pyrometer and the optical power measured. Due to the non-linear behavior of the optical power for a diode current set point under 2%, a quadratic correlation is assumed here.

3.1.2. Calibration Curve of the Pyrometer

For the correction of the temperature measured by the pyrometer T_{Pyro}, they were plotted against the measured temperature using a contact thermometer T_{real} (cf. Figure 6).

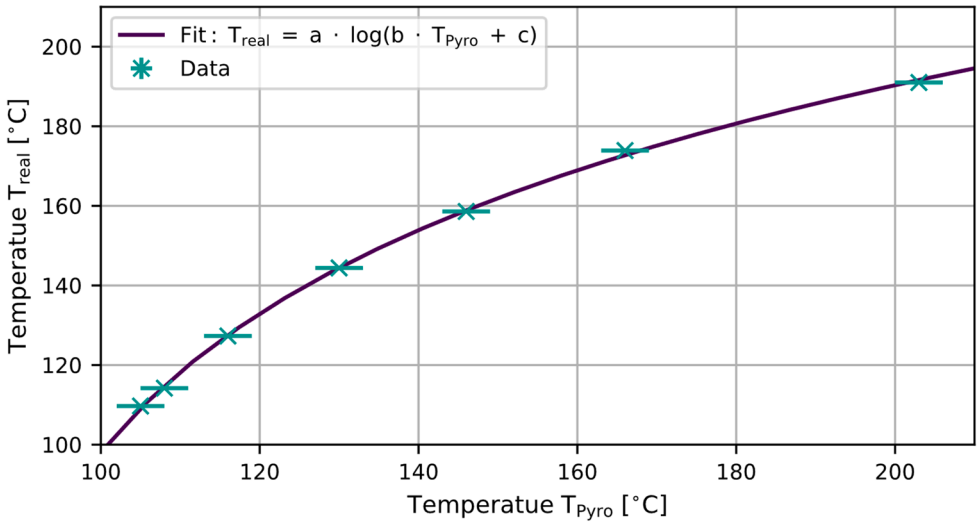

Figure 6. Calibration curve of the pyrometer for converting the measured temperatures into the temperature at the coating surface. A function of type $T_{real} = a \log(b\, T_{Pyro} + c)$ is used to fit the data.

To convert any measured values, a function of type

$$T_{real}(T_{Pyro}) = a \log(b\, T_{Pyro} + c) \tag{3}$$

was fitted to the measured data. This concrete model function was used because the logarithmic relationship describes the measured data sufficiently well, and for larger temperatures, it exhibits approximately linear behavior. This approach results in the following equation for the conversion of the pyrometer temperature:

$$T_{real}(T_{Pyro}) = 53.8\ ^{\circ}\mathrm{C} \log\left(0.28 \frac{1}{^{\circ}\mathrm{C}}\, T_{Pyro} - 22.09\right) \tag{4}$$

3.2. Measurements of the Temperature and Laser Power during Processing

For the analysis of the temperature and optical laser power, both quantities were plotted against the position "x" of the laser beam on the sample (cf. Figure 7). Furthermore, the data were broken down according to the first or second crossing of the laser (columns of Figure 7) as well as the target temperature (rows of Figure 7).

The respective control temperature was reached after a short distance (<5 mm) covered by the focused laser beam. As the control temperature increased, this distance to reach the selected temperature decreased. In addition, the measured temperature fluctuations became increasingly smaller as the selected control temperature increased. Finally, the second pass of the laser, due to less heat being needed for the polymerization and vaporization of the components, tended to require a slightly lower optical power to reach the set temperature.

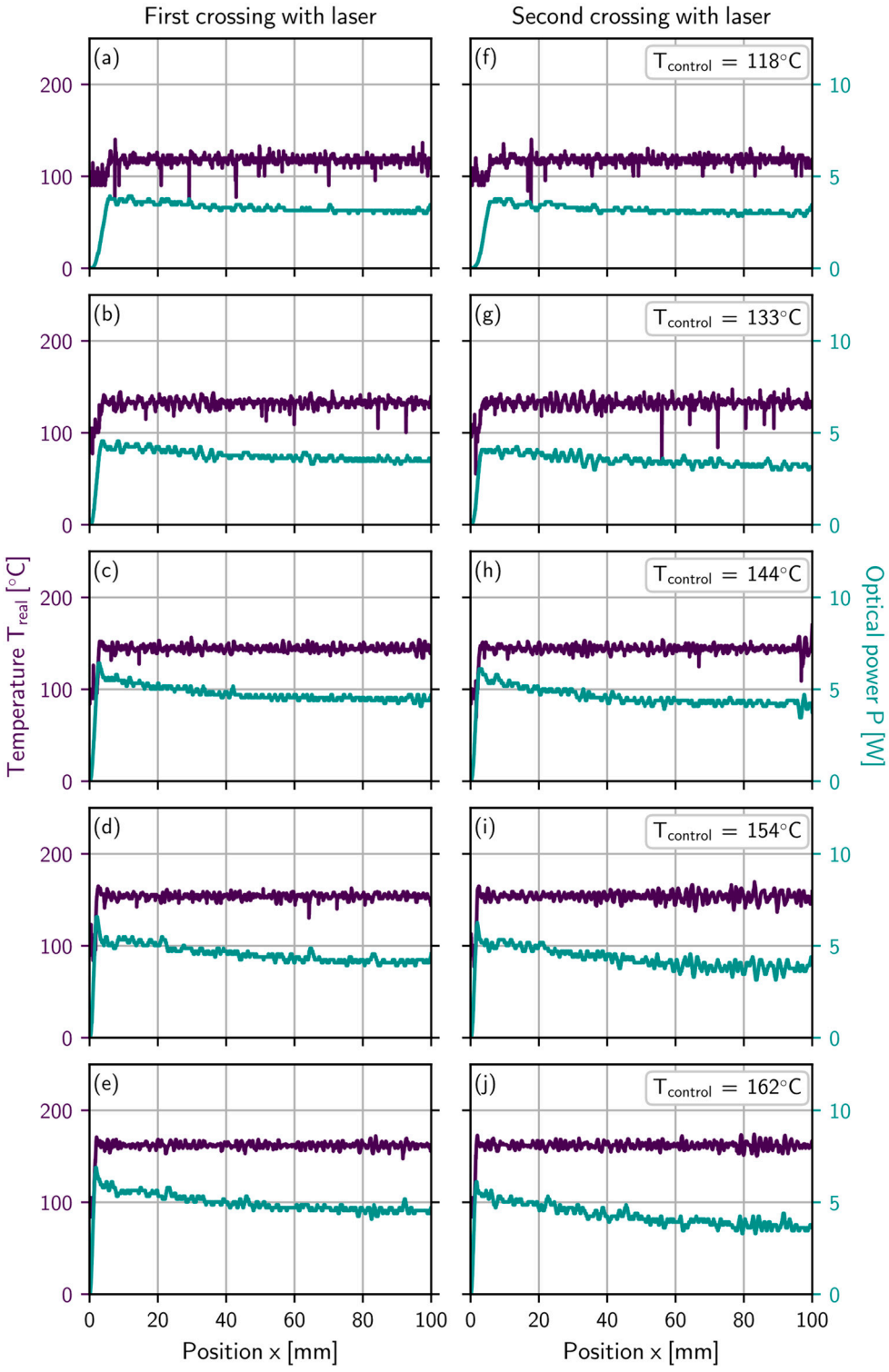

Figure 7. Measurement of the temperature and optical power of the laser during first (**a**–**e**) and second (**f**–**j**) crossing with the laser over the conductive tracks for different control temperatures at every position.

3.3. Measurements of the Electric Resistance

To analyze the relationship between the control temperature and the resulting resistance of the tracks, the two quantities are plotted against each other (cf. Figure 8). In addition, the resistance of the sample processed in the oven is plotted as a reference. When comparing the samples, it is noticeable that the samples processed by laser radiation have

a significantly lower resistance below 2 Ohms compared to 3.4 Ohms. Furthermore, the standard deviation of the measured resistances is significantly lower, both in absolute and relative terms (1.3% for oven-processed samples, <1% for laser processing, except for a set temperature of 118 °C).

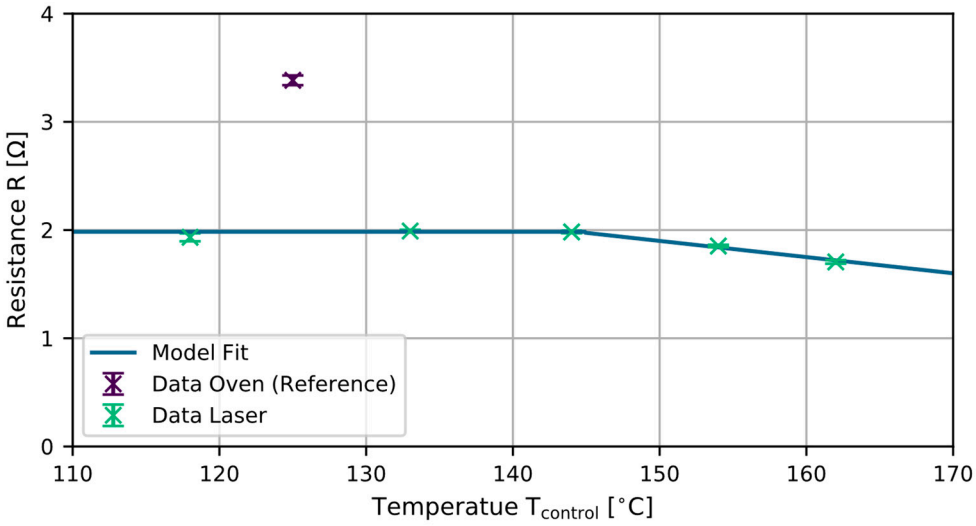

Figure 8. Resulting electrical (ohmic) resistance of the traces as a function of the set control temperature. A constant and a linear function is used to describe the resistance as a function of the temperature.

When comparing the traces processed by laser radiation, it is noticeable that up to a control temperature of approx. 144 °C, no dependence of the resistance on the control temperature can be observed. For higher temperatures, the resistance decreases approximately linearly. A function of the following form is fitted to the data:

$$R\,(T) = \begin{cases} a_0 & T_{control} < 144\ ^\circ\mathrm{C} \\ b_1 T_{real} + b_0 & T_{control} \geq 144\ ^\circ\mathrm{C} \end{cases} \tag{5}$$

This function can be used later to create tracks with a given resistance. The fit of the measured data results in the following relationship between the control temperature and electrical resistance:

$$R\,(T) = \begin{cases} 1.984\ \Omega_0 & T_{control} < 144\ ^\circ\mathrm{C} \\ -0.016\ \frac{\Omega}{^\circ\mathrm{C}} \cdot T_{real} + 4.308\ \Omega & T_{control} \geq 144\ ^\circ\mathrm{C} \end{cases} \tag{6}$$

3.4. Measurments of the Geometric Properties

To analyze the geometric properties of the tracks, the height information of the LSM measurements (cf. Figure 9a) is first averaged orthogonally to the direction of the trace (cf. Figure 9b). Then, based on this data set, linear regression is used to correct for any tilting of the substrate (cf. Figure 9c). The data processed in this way are used to determine the cross-sectional area, on the one hand, and the width of the tracks on the other. To determine the cross-section, the height information of the data is integrated using the Simpson formula. The width of the tracks is determined from the point at which the height of the trace is greater than one tenth of the maximum height of the track cross-section on both sides of the track (cf. Figure 9d).

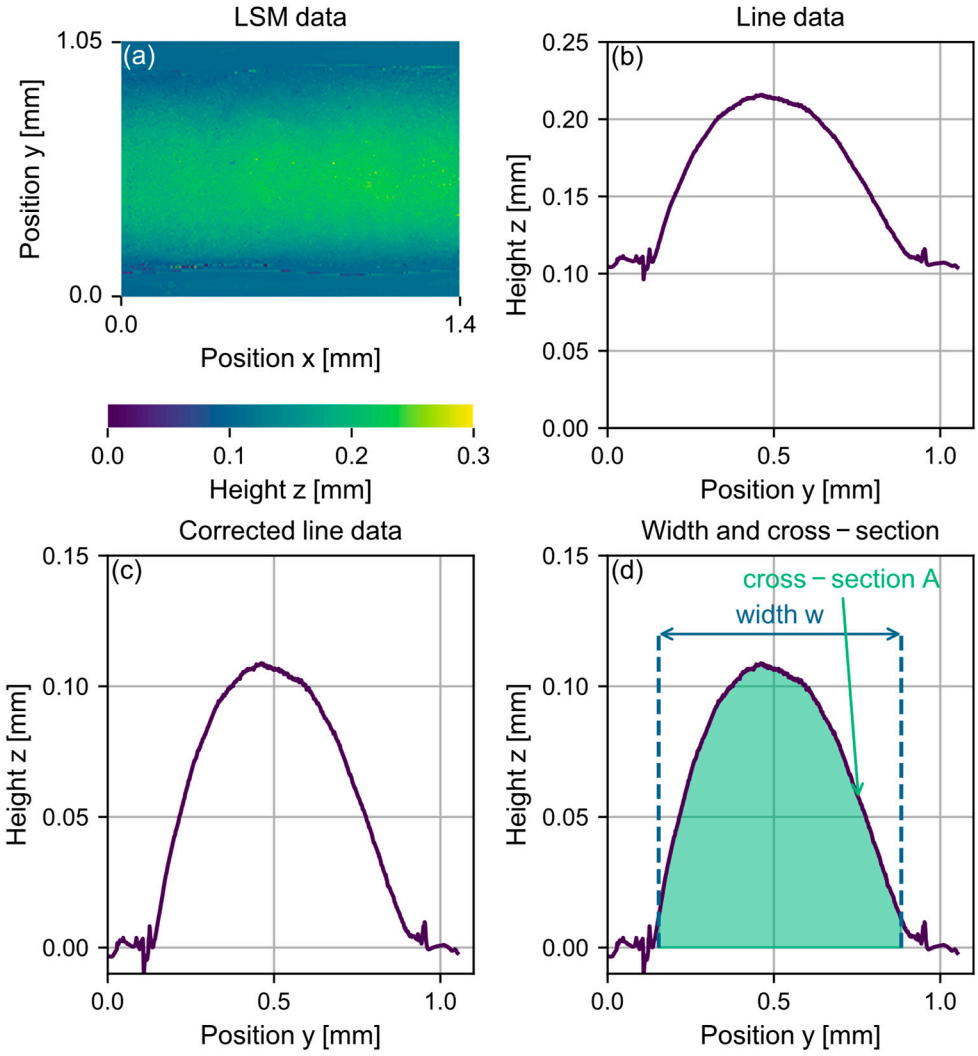

Figure 9. Method used for the analysis of the geometric properties of the cured traces: the height information from an LSM measurement (**a**) is averaged in terms of the direction x (**b**), and then corrected by linear regression (**c**). The width w or the cross-section A is determined by the difference or the integral between the first and the last points with a value of at least 0.1 z_{max} (**d**).

The values determined in this way, for the width as well as for the cross-section of the traces, are plotted as a function of the control temperature (cf. Figure 10). In addition, the width and cross-section of the conductive tracks processed in the furnace are plotted as a reference.

As a result of the evaluation, the width of the tracks is independent of the thermal treatment process (oven or laser), as well as independent of the laser processing parameters used. Nevertheless, there is a fluctuation in the values among each other. The width of the traces varies between 700 µm and 720 µm, with a standard deviation of approximately 1.5% (laser processing) to 3% (oven processing). When looking at the cross-sectional areas of the tracks, a systematic deviation in the tracks processed with laser radiation is noticeable. While the cross-section of the oven-processed tracks is 0.021 mm^2, the cross-section of the laser-processed tracks after the two laser processing steps varies between 0.045 and 0.051 mm^2, so that a difference in cross-section of approximately 200 to 250% is observed.

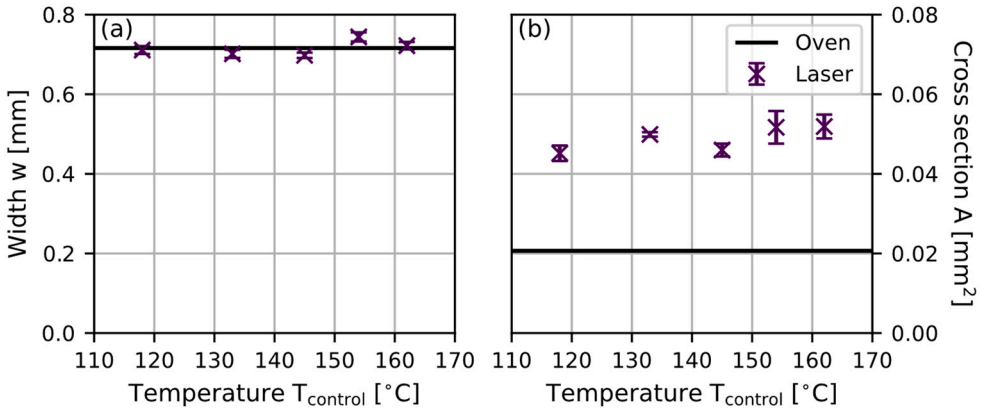

Figure 10. Results of the geometric characterization of the layers by LSM: (**a**) width of the traces as a function of the temperature, (**b**) calculated cross-section of the traces as a function of the temperature.

4. Discussion

4.1. Discussion of the Temperature and Laser Power during Processing

Based on the measurements of the temperature as well as the laser power during processing, the following assumptions can be made. Due to the initial laser radiation processing of the sample, the conductive tracks are cured close to the surface first, as the polymer matrix is superficially cured. As a result, both the electrical and thermal conductivity increase. Due to the formation of a heat front in the direction of the feed, it is necessary to reduce the laser power to maintain the set processing temperature. This curing process, which differs from the oven process, can be explained by the heat introduced into the conductive track close to the surface by the laser radiation: due to the large silver flakes, most of the laser radiation is absorbed directly at the surface of the track. Thus, on the one hand, a control temperature significantly above the glass temperature of the polycarbonate substrate can be used. On the other hand, due to the near-surface heat source, two crossings of the laser are necessary for sufficient curing of the tracks. According to experiments not described in detail here, a further increase in the number of crossings only leads to a minimal change in the electrical resistance of the conductive paths. Due to the described mechanism for thermal conduction, the interaction time between laser radiation and the conductive track is an important influencing variable on the resistivity, in addition to the control temperature (and thus the introduced energy). A longer interaction time allows the heat introduced by the laser to penetrate deeper into the conductive track. However, it should be noted here that in a potential application with a longer interaction time, the productivity of the process also decreases. The choice of two passes with a comparatively large feed rate proves to be a compromise in this potential conflict of objectives. Additional studies on various combinations of the number of passes and the feed rate still offer opportunities for optimization here.

The fact that less laser power is required during the second processing step, depending on the control temperature used, can be explained by the interaction of three mechanisms. On the one hand, the surface of the conductive track is heated more quickly, since no more energy is required for the surface curing of the conductive track. On the other hand, the higher thermal conductivity of the track, which has already been processed once, means that the heat introduced is dissipated faster on the surface. Finally, heat is also dissipated from the printed conductive track by the curing of the lower parts of it. Overall, for the two highest control temperatures considered, the effect mentioned first predominates, so that noticeably less laser power must be used here. This is in agreement with the measurement described in Section 3.3, since a clear drop in the measured resistance was shown for these parameters.

Lastly, it should be mentioned that the control loop can be further optimized. Thus, although the target control temperature is maintained on average, there are strong fluctuations in the measured temperature, especially for low temperatures. One reason for this

may be the low measured temperature, since the pyrometer operates at the lower limit of the specified measuring range and the thermal radiation emitted by the conductive track in the spectral band of the pyrometric sensor is comparatively low. Furthermore, there is potential for optimization regarding the control parameters. The single set of control parameters used in this work is aimed at the widest possible field of application regarding the control temperatures for both passes with the laser beam. However, this has the disadvantage that they are chosen too conservatively for low temperatures (recognizable by the time until the control temperature is reached—for example, at a temperature of 118 °C, cf. Figure 7a,f) and too aggressively for high temperatures (recognizable by overshoots—for example, at a temperature of 162 °C, cf. Figure 7e,j). For further tests to evaluate other influencing variables in the process, the control parameters must therefore be optimized depending on the selected control temperature.

4.2. Discussion of the Electric Resistance and Geometric Properties

Based on the measured electrical resistance, two different regimes of the process can be identified: one for a control temperature of up to 144 °C and one for a control temperature of 144 °C and higher.

For the first regime (up to 144 °C), it is noticeable that the resistance is constant when using increasing processing temperatures. Since the corresponding resistance of the conductive tracks is approximately 40% lower compared to the oven-processed sample, it can be assumed that curing in this regime is self-limiting during the laser processing of the conductive tracks. A possible reason for this is an insufficient interaction time between the laser beam and the conductive track. Due to the comparatively low thermal conductivity in the propagation direction of the laser radiation, the layers are cured, but the average distance between the particles does not change significantly, resulting in a constant electrical resistance.

For the second regime (higher than 144 °C), the resistance of the tracks decreases for increasing control temperatures. The decrease in resistance with the further increasing control temperature is due to the further curing, polymerization or decomposition of the layer. This further reduces the average distance between the particles, which in turn reduces the electrical resistance. This is possible because there is a larger thermal gradient due to the greater laser power, favoring heat conduction even at low thermal conductivity.

It should be noted that the electrical resistance has only been measured over the entire trace. However, this does not capture the effects of local temperature variations during the process on local resistance. Likewise, a possible gradient of the resistance orthogonal to the feed direction of the laser beam as a result of the non-uniform intensity profile cannot be measured in this way. It can be assumed that due to the relatively low standard deviation of the total resistance, no large fluctuations occur here. However, to verify this hypothesis, locally resolving methods of resistance measurement can be used—for example, eddy current measurements and measurements based on terahertz radiation [20–22]. Looking at the geometric properties of the traces, it is striking that while the width of the traces is independent of the type of processing, the geometric cross-section increases by 200 to 250%. Based on the microscopic images taken with the LSM, this circumstance can be explained as follows. Due to the near-surface heat source induced by the laser radiation, the upper part of the layer is cured first. The reaction products generated during the curing of the lower layer cannot escape through the already cured part of the layer and either generate gas bubbles or diffuse to the edges of the trace and condense there. Both can be clearly identified in the images of the traces processed by laser radiation compared to a trace processed in the oven (cf. Figure 11).

For further analysis of this behavior, cross-section polishes of the samples were prepared and SEM pictures were taken (cf. Figure 12). Based on these images, gas inclusions occurred for laser-processed samples, but not for the oven-processed sample. For the laser-processed samples, these gas inclusions are visible in the conductive path and below the conductive path. This confirms the hypothesis that the larger cross-section of the layers

is due to gas inclusions. It is worth mentioning that with a simple tape test, no difference in the adhesion of the traces could be detected.

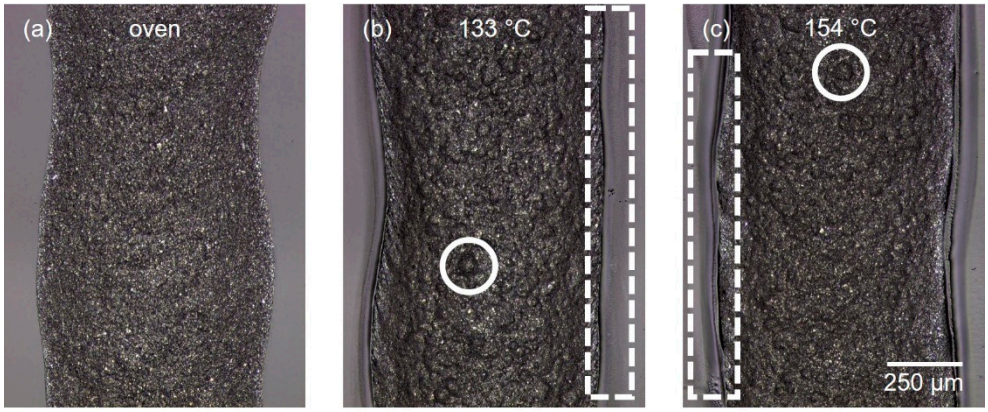

Figure 11. Comparison of the pictures recorded by LSM: (**a**) oven-processed, (**b**) laser-processed with a set temperature of 133 °C, (**c**) laser-processed with a set temperature of 154 °C. The white circles mark gas bubbles that were generated in the layer and did not escape; the white dashed rectangles show condensed residues of the solvents on the substrate surface.

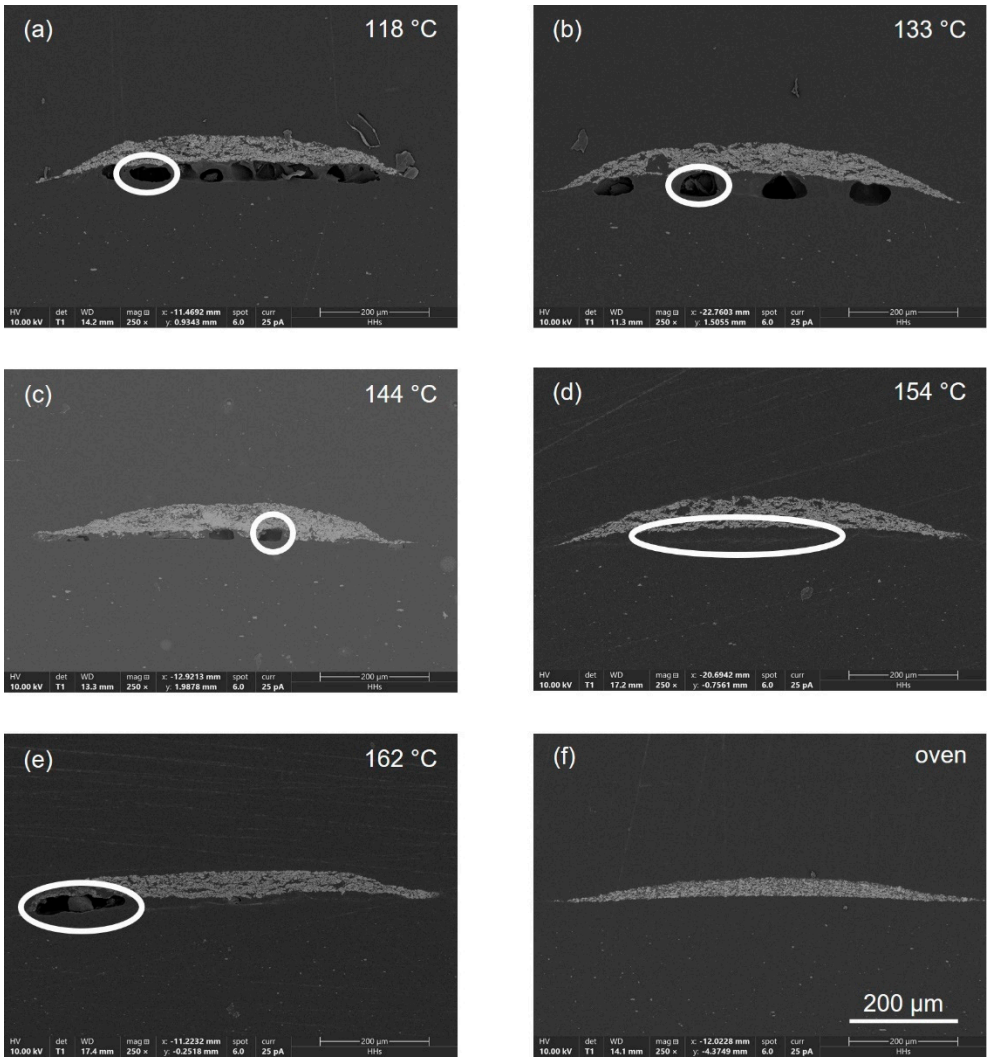

Figure 12. SEM images of cross-section polishes of the fabricated traces: laser-processed with a set temperature of (**a**) 118 °C, (**b**) 133 °C, (**c**) 144 °C, (**d**) 154 °C, (**e**) 162 °C; (**f**) oven-processed. Air inclusions due to laser processing are shown in white.

Due to the gas inclusions, the measured cross-section of the tracks was homogeneously enlarged over the entire width of the track. Since these gas inclusions can be assumed to be electrically isolating, the lower resistance of the tracks measured must be due to a different mechanism. The formation of elemental carbon during the laser processing of the layers can be ruled out as a reason for the low resistance. Carbon has a very high absorption capacity for electromagnetic radiation over a wide spectral range and would lead to hotspots and the destruction of the layer as soon as it is formed. We assume that when a laser beam is used as a heat source, the average spacing of the silver flakes is smaller and thus the resistance decreases. The smaller average distance can be explained either by the compression of the remaining material or by the additional decomposition of the polymer. However, no reliable statement can be made about this based on the SEM images taken.

Finally, it should be mentioned that based on this digitally controllable process, different electrical conductivity values can be set on individual parts of the conductive track. This is possible due to the linear relationship between the control temperature and electrical resistance for temperatures >144 °C, as well as the low variance of less than 1%.

5. Conclusions and Outlook

In this work, a two-step process for the direct application of electrically conductive tracks on polycarbonate substrates was presented. In the first step, a paste consisting of a polymer and silver flakes is applied to the substrate with a jet dispenser, and the printed conductive track is, in a second step, cured in a temperature-controlled manner with diode laser radiation treatment. The components used for this purpose were characterized and models were developed to describe the relevant parameters of temperature and optical power. Based on these results, the relationship between the set control temperature and the resulting resistance was investigated. For this purpose, in addition to measuring the resistance, the geometric properties of the traces and the power and temperature curves during processing were compared with each other and with a reference from a furnace process.

As a result, the tracks produced by means of the two-step laser-based process have a 40 to 50% lower ohmic resistance as well as a significantly lower standard deviation of the resistance of approximately <1% in comparison to samples that have been cured in an oven. Two different regimes occur when processing conductive tracks with the laser: up to a control temperature of 144 °C, no change in electrical resistance was observed. For higher temperatures, the resistance decreased linearly. In contrast, the cross-section of the laser-processed traces increased to 200 to 250%. The reason for this was identified as gaseous inclusions of the curing products in the layer. The width of the traces remains unchanged and is independent of the type of processing (oven or laser).

Based on the results presented in this paper, there are several issues to be investigated. The first is the further investigation of the process regarding the optimization of the control parameters, as well as the influence of the feed of the laser beam. Likewise, it is necessary for practical application to investigate the long-term stability of the tracks. In particular, this applies to the gas inclusions in the conductive tracks. An investigation of how these inclusions can be prevented by process technology is a relevant link to this work, too. Further, the adhesion of the traces should be systematically investigated—for example, by a cross-cut test on large-area coated surfaces instead of single tracks. Moreover, the homogeneity of the resistance has to be investigated with appropriate, locally resolving measurement methods—for example, eddy current measurements or terahertz measurements. Finally, the results can be used to develop processes in which either inhomogeneities in conductive tracks can be specifically created (for example, as a heating element) or process-related inhomogeneities (for example, from the printing process) can be eliminated.

Author Contributions: Conceptualization, J.M. and C.V.; methodology, J.M. and J.S.; formal analysis, J.M. and T.R.; investigation, J.M. and T.R.; writing—original draft preparation, J.M.; writing—review and editing, C.V., T.R. and J.S.; visualization, J.M.; supervision, C.V. and J.S.; project administration, J.M. and C.V.; funding acquisition, C.V. and J.S. All authors have read and agreed to the published version of the manuscript.

Funding: This research was funded as part of the internal programs of the Fraunhofer-Gesellschaft, the lighthouse project "GoBeyond 4.0".

Institutional Review Board Statement: Not applicable.

Informed Consent Statement: Not applicable.

Data Availability Statement: The data presented in this study are available on request from the corresponding author.

Acknowledgments: We would like to thank Philipp Dobeleit and Nataliia Matvieieva of the Fraunhofer Institute for Machine Tools and Forming Technology IWU for their help with the preparation of the samples.

Conflicts of Interest: The authors declare no conflict of interest.

References

1. Neugebauer, R. *Digital Transformation*; Springer: Berlin/Heidelberg, Germany, 2019.
2. Gu, D.; Shi, X.; Poprawe, R.; Bourell, D.L.; Setchi, R.; Zhu, J. Material-structure-performance integrated laser-metal additive manufacturing. *Science* **2021**, *372*, eabg148. [CrossRef]
3. Schmidt, R.; Möhring, M.; Härting, R.-C.; Reichstein, C.; Neumaier, P.; Jozinović, P. Industry 4.0—Potentials for Creating Smart Products: Empirical Research Results. In Proceedings of the Business Information Systems, 18th International Conference, BIS 2015, Poznań, Poland, 24–26 June 2015; Abramowicz, W., Ed.; Springer International Publishing AG: Cham, Switzerland, 2015; pp. 16–27.
4. Johannessen, J.-A. *The Emergence of the Fourth Industrial Revolution: An Historical Introduction to Knowledge Management and the Innovation Economy*; Emerald Publishing Limited: Bingley, UK, 2019.
5. Godlinski, D.; Zichner, R.; Zöllmer, V.; Baumann, R.R. Printing technologies for the manufacturing of passive microwave components: Antennas. *IET Microw. Antennas Propag.* **2017**, *11*, 2010–2015. [CrossRef]
6. Tsai, S.Y.; Lin, C.-C.; Yu, C.-T.; Chen, Y.-S.; Wu, W.-L.; Chang, Y.-C.; Chen, C.C.; Ko, F.-H. Screen-Printable Silver Paste Material for Semitransparent and Flexible Metal-Semiconductor-Metal Photodetectors with Liquid-Phase Procedure. *Nanomaterials* **2022**, *12*, 2428. [CrossRef]
7. Johannisson, W.; Carlstedt, D.; Nasiri, A.; Buggisch, C.; Linde, P.; Zenkert, D.; Asp, L.E.; Lindbergh, G.; Fiedler, B. A screen-printing method for manufacturing of current collectors for structural batteries. *Multifunct. Mater.* **2021**, *4*, 35002. [CrossRef]
8. Vedder, C.; Hawelka, D.; Wolter, M.; Leiva, D.; Stollenwerk, J.; Wissenbach, K. Laser-based drying of battery electrode layers. In Proceedings of the 35th International Congress on Applications of Lasers & Electro-Optics, San Diego, CA, USA, 16–20 October 2016.
9. Meixner, M.; Stollenwerk, J.; Weigt, W.; Zschuppe, M. Laser statt Trockenöfen. *Farbe Lack* **2015**, *3*, 88–92.
10. Khan, S.; Lorenzelli, L.; Dahiya, R.S. Technologies for Printing Sensors and Electronics Over Large Flexible Substrates: A Review. *IEEE Sens. J.* **2015**, *15*, 3164–3185. [CrossRef]
11. Roshanghias, A.; Krivec, M.; Baumgart, M. Sintering strategies for inkjet printed metallic traces in 3D printed electronics. *Flex. Print. Electron.* **2017**, *2*, 45002. [CrossRef]
12. Wünscher, S.; Abbel, R.; Perelaer, J.; Schubert, U.S. Progress of alternative sintering approaches of inkjet-printed metal inks and their application for manufacturing of flexible electronic devices. *J. Mater. Chem. C* **2014**, *2*, 10232–10261. [CrossRef]
13. Niittynen, J.; Sowade, E.; Kang, H.; Baumann, R.R.; Mäntysalo, M. Comparison of laser and intense pulsed light sintering (IPL) for inkjet-printed copper nanoparticle layers. *Sci. Rep.* **2015**, *5*, 8832. [CrossRef]
14. Olsen, E.; Overmeyer, L. Laser sintering of copper conductive traces on primer pre-treated additive manufactured 3D surfaces. *Flex. Print. Electron.* **2021**, *6*, 15006. [CrossRef]
15. Kinzel, E.C.; Sigmarsson, H.H.; Xu, X.; Chappell, W.J. Laser sintering of thick-film conductors for microelectronic applications. *J. Appl. Phys.* **2007**, *101*, 63106. [CrossRef]
16. Ermak, O.; Zenou, M.; Toker, G.B.; Ankri, J.; Shacham-Diamand, Y.; Kotler, Z. Rapid laser sintering of metal nano-particles inks. *Nanotechnology* **2016**, *27*, 385201. [CrossRef]
17. Joo, M.; Lee, B.; Jeong, S.; Lee, M. Laser sintering of Cu paste film printed on polyimide substrate. *Appl. Surf. Sci.* **2011**, *258*, 521–524. [CrossRef]
18. Sonoda, H.; Atsumi, R.; Mita, M.; Yamasaki, K.; Maekawa, K. On-demand laser-sintering of copper micro-particles on ferrite/epoxy resin substrates for power electronics devices. In Proceedings of the 2016 IEEE 18th Electronics Packaging Technology Conference (EPTC), Piscataway, NJ, USA, 30 November–3 December 2016; Suntec Singapore Convention & Exhibition Centre: Piscataway, NJ, USA, 2016; pp. 301–305.

19. Hernandez-Castaneda, J.C.; Lok, B.K.; Zheng, H. Laser sintering of Cu nanoparticles on PET polymer substrate for printed electronics at different wavelengths and process conditions. *Front. Mech. Eng.* **2020**, *15*, 303–318. [CrossRef]
20. Wenzel, K.; Mertin, J.; Vedder, C.; Klein, S.; Traub, M.; Kohlhaas, R.B.; Schell, M.; Globisch, B.; Liebermeister, L. Sheet Resistance Imaging on Ag Thin Films with THz-TDS in Reflection Geometry. In Proceedings of the 47th International Conference on Infrared, Millimeter and Terahertz Waves (IRMMW-THz), IEEE, Delft, The Netherlands, 28 August–2 September 2022; pp. 1–2.
21. Zhuldybina, M.; Ropagnol, X.; Blanchard, F. Towards in-situ quality control of conductive printable electronics: A review of possible pathways. *Flex. Print. Electron.* **2021**, *6*, 43007. [CrossRef]
22. Lewis, A.P.; Hunt, C.; Thomas, O.; Wickham, M. High-speed non-contact sheet resistivity monitoring of printed electronics using inductive sensors. *Flex. Print. Electron.* **2017**, *2*, 44001. [CrossRef]